JGR Atmospheres

RESEARCH ARTICLE
10.1029/2019JD031414

Key Points:
- Projected increase in sulfate emissions is expected to overcompensate carbonaceous aerosol mitigation over India
- Increase in sulfates and decrease in carbonaceous aerosols over India in the mitigation scenario is expected to decrease the ISM
- Dust transport across the Arabian Sea is expected to decrease during ISM in the mitigation scenario relative to the baseline scenario

Supporting Information:
- Supporting Information S1
- Figure S2
- Figure S3
- Figure S4

Correspondence to:
S. Das,
sdas@ictp.it

Citation:
Das, S., Giorgi, F., Giuliani, G., Dey, S., & Coppola, E. (2020). Near-future anthropogenic aerosol emission scenarios and their direct radiative effects on the present-day characteristics of the Indian summer monsoon. *Journal of Geophysical Research: Atmospheres*, *125*, e2019JD031414. https://doi.org/10.1029/2019JD031414

Received 1 DEC 2018
Accepted 31 JAN 2020
Accepted article online 3 FEB 2020

Near-Future Anthropogenic Aerosol Emission Scenarios and Their Direct Radiative Effects on the Present-Day Characteristics of the Indian Summer Monsoon

Sushant Das[1], Filippo Giorgi[1], Graziano Giuliani[1], Sagnik Dey[2,3], and Erika Coppola[1]

[1]Earth System Physics Section, The Abdus Salam International Centre for Theoretical Physics, Trieste, Italy, [2]Centre for Atmospheric Sciences, Indian Institute of Technology Delhi, New Delhi, India, [3]Centre of Excellence for Research on Clean Air, Indian Institute of Technology Delhi, New Delhi, India

Abstract Various air pollution mitigation scenarios have been proposed to improve the existing severe air quality problem over South Asia. Here we use a regional climate model to examine the response of the Indian summer monsoon (ISM) to two projected anthropogenic aerosol emission scenarios (a) short-lived climate pollutant "mitigation" scenario (2020–2030) and (b) current legislation "baseline" scenario (2005–2015). In the mitigation scenario, carbonaceous aerosol (black carbon and organic carbon) emissions are projected to decrease while sulfate emissions are projected to increase. This is expected to result in a marginal increase in anthropogenic aerosol optical depth over India (by 0.04–0.08). The dominating effect of scattering aerosols over absorbing aerosols in the mitigation scenario is expected to enhance atmospheric cooling over the Indian landmass, which in turn dampens the latitudinal thermal gradient and leads to a weakening of the ISM. This effect also reduces dust emissions over the Arabian Peninsula and transport across the Arabian Sea, decreasing the influence of the dust radiative feedback on the ISM. In addition, the increased amounts of sulfate and decreased amounts of carbonaceous aerosols are expected to result in drier conditions over the central parts of India. We also show that changes in emissions of different types of anthropogenic aerosols induce a chain of feedbacks, which can modulate the space-time variability of dust, thereby affecting the magnitude of dust radiative effects on the ISM dynamics. We conclude that it is critical from the policy point of view to implement strategies to cut the currently increasing sulfate emissions.

1. Introduction

Rapid growth in industrialization, land-use change, and other anthropogenic activities have led to a continuous rise in anthropogenic aerosol loadings over India during the last two decades (Dey & Di Girolamo, 2011; Moorthy et al., 2013). High anthropogenic aerosol emissions pose a substantial threat to society, as aerosols impact the Indian summer monsoon, or ISM (Bollasina et al., 2011), and the health of a billion-plus population [Cohen et al., 2017]. Anthropogenic aerosols are considered as short-lived climate pollutants (SLCP) because of their short atmospheric residence time (days to a few weeks) and are receiving increasing attention because they can modulate climate (Shindell et al., 2008) especially at the regional scale.

Aerosols affect climate directly by scattering and absorbing solar radiation (Giorgi et al., 2002; Haywood & Boucher, 2000) and indirectly by acting as cloud condensation nuclei and modifying the properties of clouds (Albrecht, 1989; Twomey, 1974). In addition, aerosol deposition on snow can lead to a reduction of surface albedo and can affect the thermal structure of the atmosphere through the snow-albedo feedback (e.g., Flanner et al., 2007; Jiang et al., 2017). Aerosol impacts can be in the direction of cooling or warming depending on the aerosol composition and optical properties. For example, black carbon (BC) aerosols are important contributors to global warming because of their light absorbing properties (Bond et al., 2013). On the other hand, sulfates and organic carbon (OC) are more reflective of solar radiation, and thus induce cooling [e.g., Myhre et al., 2004; Lin et al., 2014]. Both natural (e.g., mineral dust and sea salt) and anthropogenic aerosols contribute to the spatial and temporal variability of the aerosol optical depth (AOD), which also depends on local atmospheric processes, topography, and aerosol radiative feedbacks.

While reducing anthropogenic aerosol emissions reduces aerosol burdens and associated health effects, the resulting impact on the regional climate is still uncertain. Highly polluted regions, such as East Asia, suffer from major air pollution crises and have been implementing initiatives to curb down aerosol emissions (Li et al., 2017). Studies have indicated that aerosols can affect the East Asian summer monsoon by modulating its characteristics through their direct and indirect effects (Jiang et al., 2015; Liu et al., 2011). At the same time, the aerosol-induced changes in the East Asian summer monsoon characteristics depend on the type of anthropogenic aerosols species. For example, Jiang et al. (2013) found that anthropogenic sulfates and primary organic matter suppress precipitation in North China, while the effect of BC on precipitation is relatively small.

Many studies have demonstrated the capability of aerosols to modulate the ISM characteristics; however, the argument of whether aerosol forcing decreases or increases the intensity of the ISM is still a matter of debate. The ISM produces nearly 80% of annual precipitation over India in the period of June–September and has a huge societal impact because of India's reliance on an agriculture-driven economy. Various hypotheses have been proposed concerning aerosol-ISM interactions. Ramanathan et al. (2005) suggested that the presence of aerosol-induced cooling (through solar dimming) over the northern Indian Ocean weakens the land-sea thermal contrast, resulting in a weakening of the ISM. Bollasina et al. (2011) also supported this argument, while Menon et al. (2002) concluded that the presence of BC could lead to both increases or decreases of the ISM intensity over different subregions of India.

In addition, the response of the ISM to aerosol forcings depends on fast and slow feedback processes (Ganguly et al., 2012a). Lau and Kim (2006) proposed the "elevated heat pump" hypothesis, whereby absorbing aerosols (e.g., mineral dust an BC) induce a latitudinal gradient in tropospheric heating over the ISM region during the premonsoon season resulting in an early arrival of the ISM. Vinoj et al. (2014) found a strengthening of the ISM circulation due to large-scale convergence induced by dust over the Arabian Peninsula.

Most aerosol-ISM interaction studies mentioned above have been carried out using global climate models (GCMs) at coarse resolutions, which have limitations in resolving the physical mechanisms associated with the aerosol-ISM interactions. Moreover, aerosol emissions occurring at local scales and topographical details may not be well represented in coarse resolution GCMs. Regional climate models (RCMs) can thus be useful tools to study aerosol-climate interactions due to their ability to reach finer resolutions (Giorgi, 2019). On the other hand, RCMs cannot take into account the teleconnections and global adjustments to regional perturbations, which is another important factor in determining aerosol induced regional climate effects (Bollasina et al., 2011), but they can capture regional adjustments derived from aerosol forcings, which can play a primary role over particular regions (e.g., Ramanathan et al., 2005).

Indeed, RCMs are increasingly being used to examine aerosol-ISM interactions. For example, Solmon et al. (2015) used the RegCM model coupled to an aerosol module (Solmon et al., 2006; Zakey et al., 2006) to provide strong evidence of important relationships between the increasing trend of Arabian dust activity and the ISM. *Das et al.* [2015b] found that the ISM strengthens in response to a stronger dust radiative feedback due to enhanced absorption of incoming solar radiation. Similar conclusions were drawn by Jin et al. (2016) using the WRF-Chem model. Furthermore, it has been shown that if only anthropogenic BC, OC and SO_2 are considered, the ISM is weakened due to increased surface pressure over landmass that inhibits the southwest monsoon wind flow (Das et al., 2016).

It is thus evident that the aerosol impacts on the ISM dynamics depend on the composition and relative burdens of different aerosol types, and on the interactions between aerosols of natural and anthropogenic origin. Since different emission mitigation measures might affect the overall relative burden of anthropogenic aerosols, it becomes important to understand how air pollution mitigation measures envisioned for the future might modify the ISM circulation and regional climate. Based on these considerations, here we analyze the response of the ISM to changes in anthropogenic aerosol emissions for different scenarios developed by the Evaluating the Climate and Air Quality Impacts of Short-lived Pollutants (ECLIPSE) project (Baker et al., 2015; Stohl et al., 2015).

Toward this goal, we use a RCM—the RegCM4 (Giorgi et al., 2012), developed at the Abdus Salam International Centre for Theoretical Physics—coupled to an aerosol module including OC, BC, sulfates, mineral dust, and sea spray (Solmon et al., 2006; Zakey et al., 2006; Zakey et al., 2008). The ECLIPSE inventory provides global emission fields for current legislature ("baseline" scenario), SLCP "mitigation" scenarios, and no further control scenario. For the baseline scenario, the anthropogenic emissions are for the period 2005–2015 and for the mitigation scenario, the anthropogenic aerosol emissions are provided for the near-future period of 2020–2030.

To isolate the effect of anthropogenic aerosols on the ISM characteristics, we use these different emission scenarios within the same driving meteorological boundary conditions, which are derived for the period 2005–2015 from the ERA-Interim reanalysis of observations. Also, to assess the effects of different aerosol types we intercompare a set of sensitivity experiments for the same period including only the individual anthropogenic aerosol components. Before discussing the results of our study, more information on the model, anthropogenic emission inventories, and sensitivity experiment design is provided in the next section.

2. Methodology and Data

2.1. RegCM4 Physics, Configurations, and Boundary Conditions

For the present study, we use the International Centre for Theoretical Physics RCM RegCM Version 4 (RegCM4, Giorgi et al., 2012), which has been extensively used to study regional climate change and processes across various CORDEX domains (Co-ordinated Regional Climate Downscaling Experiment; Giorgi et al., 2009). In brief, RegCM4 is a limited area, sigma vertical coordinate hydrostatic model with an Arakawa B horizontally staggered grid and a time-splitting explicit integration scheme. The model includes the community land surface model—CLM4.5 (Oleson et al., 2013)—to represent land surface processes and exchanges with the atmosphere.

RegCM4 is coupled with an online aerosol tracer module (Solmon et al., 2006; Zakey et al., 2006; Zakey et al., 2008), which follows surface emissions, advection, horizontal and vertical turbulent diffusion, convective transport and dry and wet deposition. Natural aerosols such as mineral dust and sea salt are described using a bin representation with size ranging between ~0 and 20 μm (four bins) for mineral dust and ~0 and 10 μm (two bins) for sea salt. The dust mobilization is due to the wind characteristics over land built in the CLM4.5 land module (Oleson et al., 2013). Important factors include the frictional wind speed, vegetation cover and soil moisture, which determine the soil erodibility and dust emission. The dust mobilization scheme follows physical parameterization processes based on the Dust Entrainment and Deposition scheme (Zender et al., 2003). Sea salt emissions are generated based on a threshold wind velocity over the sea following Zakey et al. (2008). Anthropogenic aerosols include BC, OC, and sulfates, that is, SO_2 and its aqueous particle conversion to SO_4 (Qian et al., 2001). Both the hydrophobic and hydrophilic components of BC and OC are considered. Details of the anthropogenic aerosol inventory are given in the next section. Both natural and anthropogenic aerosols (12 tracers) and their direct effects are considered in the model simulations, while indirect effects on cloud characteristics are not yet included in the model.

Concerning the other model physics parameterizations, we use the UW-PBL boundary layer scheme (Grenier & Bretherton, 2001), the MIT convection scheme [Emanuel & Zivkovic, 1999] over land and Tiedtke scheme (Tiedtke, 1989) over ocean, respectively. Atmospheric radiative transfer processes are described in (Kiehl et al., 1996), while the large-scale precipitation from nonconvective clouds is represented through the Subgrid Explicit Moisture Scheme (Pal et al., 2000) and the ocean flux parameterization is based on Zeng et al. (1998). The model employs a 50-km horizontal grid spacing over the South Asia CORDEX domain (Figure 1a), which is sufficiently large for examining aerosol induced regional climate adjustments. The model uses 23 vertical levels with the top at 50 hPa. Land type and topography are taken from the United States Geological Survey (USGS) data set at 30 seconds resolution. The atmospheric lateral boundary conditions necessary to run the simulations are provided from the ERA-interim (EIN15) reanalysis data set (Dee et al., 2011) with $1.5° \times 1.5°$ resolution and are updated every 6 hr. Optimum interpolated weekly sea surface temperature (SST) gridded data at $1° \times 1°$ resolution are used as provided by the National Oceanic and Atmospheric Administration. The lateral boundary conditions for aerosols are prescribed from global runs performed using the CAM-Chem model (Solmon et al., 2015).

2.2. Anthropogenic Emission Inventory

The ECLIPSE emission database (Stohl et al., 2015) used in this work was generated by the Greenhouse gas Air pollution Interactions and Synergies model, which considers different sectors such as energy consumption, economy, and technological intervention. Here we use the ECLIPSE emission Version 5a available at 50-km resolution for two scenarios: (i) the current legislature (CLE) “baseline scenario” for the period of 2005–2015 and (ii) SLCP “mitigation scenario” for the near-future period of 2020–2030. The baseline

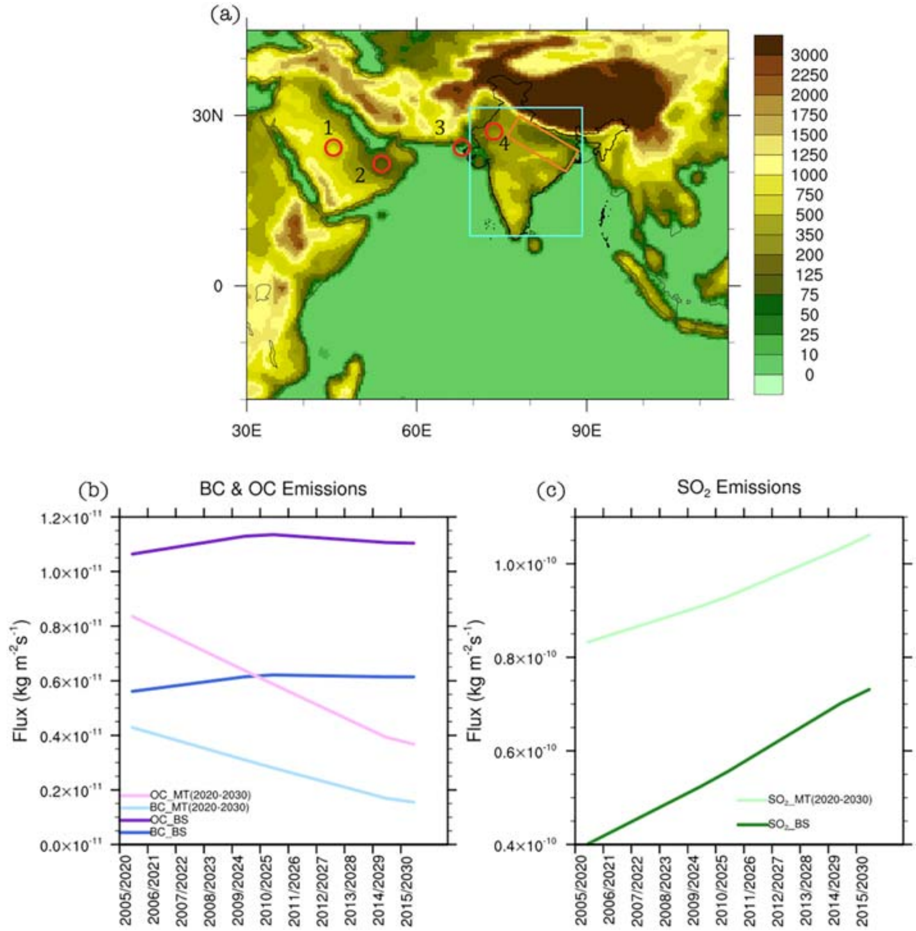

Figure 1. (a) South Asia CORDEX Domain and shaded color showing the topography (m) at 50-km resolution. Time series of annual mean emissions ($kg{\cdot}m^{-2}{\cdot}s^{-1}$) of (b) carbonaceous aerosols (BC and OC) and (c) SO_2 for the baseline period (2005–2015) and mitigation period (2020–2030) averaged over India as demarcated by cyan box (7–30°N and 70–88°E). The red color circles in Figure 1a represent the AERONET stations with numbered (1) Solar Village, (2) Meziara in Arabian Peninsula, (3) Karachi in Pakistan, and (4) Jaipur in India. The orange rectangular box represents Indo-Gangetic Basin (IGB).

emissions are based on current and existing government regulating laws in the respective countries whereas the mitigation scenario is obtained assuming the implementation of climate-related policies aimed at curbing down future anthropogenic emissions.

In our study, we include three anthropogenic SLCPs, that is, BC, OC, and SO_2. All the SLCP emissions from different sources are available at 5-year intervals with prescribed monthly weights. The data are first used to build time series of total emissions for each species taking into account agricultural burning, residential and commercial emissions, power plants with energy conversion and extraction, industrial combustion with processing, surface transportation, waste management, and shipping emissions. Monthly weights (β) for the independent sources (α) are used to generate seasonality for each 5-year time period. The total emissions (E) and seasonality for each species are computed following $\sum_{\substack{1\le\alpha\le7\\1\le\beta\le12}} E(\alpha,\beta)$, where α varies from 1 to 7 depicting emissions from different categories and β represents the monthly weights from January to December in each of the grids. Note that every emission inventory has uncertainty (e.g., Gadhavi et al., 2015; Nair et al., 2012; Zhao et al., 2011) in various parameters that are used to compute emissions, and all sources may not be possibly considered.

The annual mean anthropogenic emissions of SLCP in the baseline and mitigation scenarios averaged over India are shown in Figures 1b and 1c. Emissions of carbonaceous aerosols (BC and OC) are expected to be reduced drastically (~2–5 times) in the mitigation scenario. However, this is not the case for SO_2, which

Table 1
List of Experiments Carried Out Considering Different Aerosol Species Under Different Anthropogenic (BC, OC, and Sulfates) Aerosol Emission Scenarios

Ser. No.	Name	Species	Radiative interaction	Anthropogenic emissions scenarios
1	Total_CTL	BC, OC, sulfates, dust, and sea salt	No/transport only	Baseline
2	Carb_BS	BC and OC	Yes	Baseline
3	Carb_MT	BC and OC	Yes	Mitigation
4	Suca_BS	BC, OC, and Sulfates	Yes	Baseline
5	Suca_MT	BC, OC, and Sulfates	Yes	Mitigation
6	Total_BS	BC, OC, sulfates, dust, and sea salt	Yes	Baseline
7	Total_MT	BC, OC, sulfates, dust, and sea salt	Yes	Mitigation

Note. The baseline denotes anthropogenic aerosol emissions for the period of "2005–2015," and mitigation denotes anthropogenic aerosol emissions for the period of "2020–2030."

shows a rapid increase in the near future by a factor of ~2–3, resulting in increased sulfate loadings over India. One of the key reasons for the decrease in BC is the shift to cleaner modes of residential usage, especially over rural areas (Rana et al., 2019). Other ways of BC mitigations over India are summarized in Rana et al. (2019), and references therein. The spatial differences in annual emissions of BC, OC, and SO_2 between mitigation and baseline scenarios over India are shown in Figure S1 in the supporting information. Consistent with the ECLIPSE inventory, Li et al. (2017) reported an increase in the SO_2 emissions over India based on Ozone Measuring instrument data, and attributed it to the increased use of coal-fired energy in power plants and industries.

2.3. Experiment Design

The model is integrated for the 11-year period from 1 January 2005 to 31 December 2015, and the analysis is carried out for the period 2006–2015 (10 years) considering the initial year as spin up. In the first part of the study, experiments were carried out with only anthropogenic aerosols for each scenario, as summarized in Table 1. In the baseline control experiment (hereafter, Total_CTL) the aerosols are not allowed to interact with the radiation. Then, we first consider only radiatively interactive carbonaceous aerosols in both emission scenarios (Carb_BS and Carb_MT), and subsequently radiatively interactive sulfate and carbonaceous aerosols (Suca_BS and Suca_MT). After investigating the impacts of all anthropogenic aerosols on the ISM under both scenarios, we include the natural aerosol (dust and sea salt) radiative effects in the simulations (Total_BS and Total_MT) (see Table 1 for more details). The differences obtained from the Carb_BS and Carb_MT relative to Total_CTL and Suca_BS and Suca_MT relative to Total_CTL provide the responses of the ISM to emissions of carbonaceous aerosols and net anthropogenic aerosols, respectively. The differences obtained from the Total_BS and Total_MT relative to Total_CTL provide the total aerosol impacts including dust and sea-salt radiative effects. Here, we want to specify that the boundary conditions are the same in all the experiments in order to isolate the effects of aerosols. Only changes in the anthropogenic aerosol (BC, OC, and SO_2) emissions are considered for the different scenarios, that is, baseline for 2005–2015 and mitigation for 2020–2030, respectively.

3. Results

3.1. Evaluation of the Model Performance

First, we evaluate the model performance in simulating precipitation, winds and AOD during the summer monsoon season. The spatial distributions of mean precipitation (shaded) from the Global Precipitation Climatology Project observations and RegCM simulation (Total_CTL case) during the ISM season for the period 2006–2015 are shown in Figures 2a and 2b. The Global Precipitation Climatology Project Version 3.0 data are available at $0.5° \times 0.5°$ resolution around the globe and are derived from multiple satellites and rain gauges (Huffman et al., 2019). Despite the presence of some biases, the model simulates the spatial distribution of observed precipitation patterns reasonably well, with maximum precipitation (>10 mm/day) over the northeast hilly regions as well as parts of the Western Ghats. Among the main biases is an underestimation of precipitation by 2 to 6 mm/day over some central regions of India (Figure 2c). This problem is however common to many global and regional models over the Indian subcontinent, and in fact, our model performance is in line with most previous studies (Mishra et al., 2018; Singh et al., 2016; Sperber et al., 2013).

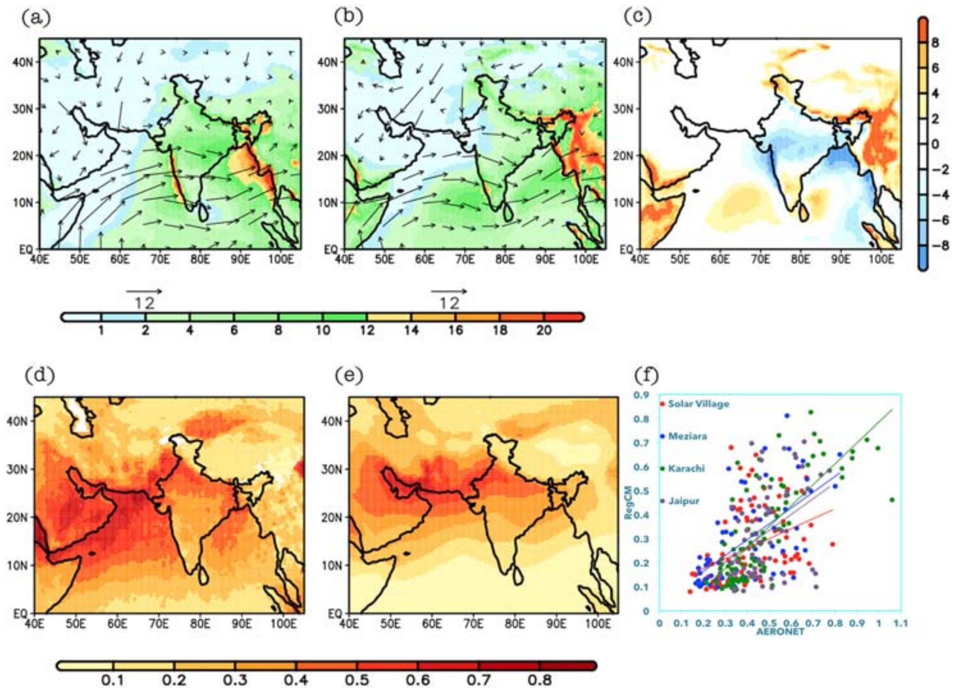

Figure 2. Spatial distribution of mean summer monsoon (June–September) precipitation (shaded in mm/day) and winds (vector in m/s) at 850 hPa derived from (a) GPCP and EIN75, (b) RegCM (Total_CTL case), and (c) precipitation bias (Model-GPCP). Spatial distribution of mean total aerosol optical depth derived from (d) MISR and simulated by (e) RegCM (Total_CTL case) during the summer monsoon seasons of the period 2006–2015. Figure 2f Scatter plot between the available monthly averaged AOD data retrieved by different AERONET stations at 550 nm and RegCM within the simulation period 2006–2015. The stations are marked in Figure 1a.

This dry bias may be associated with reduced soil moisture availability simulated by CLM4.5 (Maharana et al., 2019).

It is also to be noted that dynamical downscaling is sensitive to the selection of different physics and boundary conditions over a specific domain (Giorgi et al., 2012; Raju et al., 2015), and the RegCM model has been extensively used to simulate the ISM features such as characteristics of precipitation patterns and wind circulations (e.g., Dash et al., 2006; Dash et al., 2013). In particular, the model is quite able to capture the spatial distribution of southwest winds at 850 hPa over the Indian subcontinent, also known as the monsoon low-level jet (vectors in Figures 2a and 2b). It simulates maximum wind speed over the Arabian Sea, which is an important feature in transporting moisture from the Arabian Sea toward the Indian landmass. Comparison against the EIN75 reanalysis data shows that the simulated low-level winds are slightly weaker than in EIN75, and this can be a further contribution to the dry bias over central India (Ghosh et al., 2019).

In terms of aerosol studies, RegCM has been widely used by the modeling community, for example, over Africa (Solmon et al., 2012; Tummon et al., 2010), East Asia [Giorgi et al., 2002; Sun & Liu, 2015; Yin et al., 2015], and Europe (Solmon et al., 2006; Zanis et al., 2012). Concerning South Asia, Nair et al. (2012) investigated the seasonal variation of BC aerosols over India, while Das, Dey, Dash (2015), Das, Dey, Dash, Giuliani, et al. (2015) examined the direct aerosol radiative feedback on the ISM.

The spatial distributions of mean summer monsoon total AOD from the model experiment Total_CTL and the Multiangle Imaging SpectroRadiometer (MISR) are shown in Figures 2d and 2e. The level 3 MISR AOD is available at 0.5° × 0.5° resolution at 555 nm, and has been extensively used for aerosol climatological studies over the Indian subcontinent (e.g., Dey & Di Girolamo, 2010). The model simulates the high regional aerosol hotspots (total AOD > 0.6) over the Thar Desert and Indo-Gangetic Basin (IGB). Qualitatively, the major dust sources in the Middle East, that is, deserts over Saudi Arabia, Oman, Iran, Iraq, and Afghanistan are captured; however, the dust amounts are underestimated in the southern parts of the Arabian Peninsula and Arabian Sea by 0.1 to 0.2. This can be attributed to an underestimation of near surface winds over these regions (Zakey et al., 2006). Also, the dust source emission scheme is very sensitive to the soil parameters, which can strongly influence model biases. In addition, the model underestimates the total AOD over parts of the central to eastern IGB and over the northern Bay of Bengal, where the outflow of aerosols from the Indian continent occurs due to the prevailing wind circulations (Tiwari et al., 2016). On the other hand, the IGB also consists of some anthropogenic aerosol species that are not considered in the model, such as secondary OC aerosols, inorganic aerosols, and brown carbon (Chakraborty et al., 2016). This can clearly contribute to the underestimation of AOD compared to MISR data.

Nair et al. (2012) found a smaller discrepancy between observed and simulated BC aerosols during the summer monsoon season compared to the winter season. Concerning desert dust, RegCM has been previously shown to capture the seasonality of dust sources and transport over the Indian subcontinent (Das et al., 2013). Their study found that the dust transport initiates during the premonsoon season (March–May) while maximum dust loads occur during the mature monsoon season, with most of dust getting transported at ~700–850 hPa over the IGB. Recent studies have suggested potential impacts of Middle East desert aerosols in modulating the ISM dynamics and intraseasonal variability (Jin et al., 2015; Vinoj et al., 2014), and indeed, mineral dust was found to dominate over anthropogenic aerosols in total aerosol loading during the monsoon season over the Indian subcontinent (Dey & Di Girolamo, 2010). Jin et al. (2018) also found a major contribution of dust (~60–80%) in the total summer AOD over the Middle East and India using several sets of observation data.

The monthly AOD values from the Total_CTL case are further validated against AOD retrieved from the ground-based Aerosol Robotic Network (AERONET) at 500 nm across the domain. AERONET Version 3—Level 2 AOD data at stations Solar Village, Meziara, Karachi, and Jaipur are analyzed for this purpose. Details about the stations selected, which are close to the desert sources and away from major urban centers characterized by aerosols not included in the model, and the retrieval technique can be found in Dubovik et al. (2002). Correlation coefficients (R) of 0.40, 0.62, 0.76, and 0.42 between simulated and AERONET monthly AOD values (Figure 2f) are found at Solar Village, Meziara, Karachi, and Jaipur, respectively, with an overall value of $R = 0.58$, implying a good model performance.

To summarize, although the model in its present configuration underestimates AOD over certain regions, also because of the lack of some anthropogenic aerosol types, it replicates the spatial distribution of the observed total AOD and its north-south gradient over the Indian subcontinent during the ISM season. Note that there are also uncertainties involved in the observational AOD data sets used, that is, AERONET and MISR. For example, the Indian subcontinent is substantially covered with thick clouds during the ISM and therefore the retrieval of AOD information could be potentially contaminated (Giles et al., 2019; Kahn et al., 2010). Overall, given all the sources of uncertainty in aerosol emissions and observations, and the lack of some anthropogenic aerosol types, this assessment gives us confidence that the model can realistically simulate the impacts of aerosol radiative feedbacks on the ISM.

3.2. Anthropogenic Aerosol Feedbacks on the ISM Under the Baseline and Mitigation Scenarios

Seasonal mean anthropogenic AOD during the ISM derived from the Carb_BS, Carb_MT, Suca_BS, and Suca_MT experiments is shown in Figure 3. The anthropogenic AOD is lower in the mitigation scenario than in the baseline scenario when only carbonaceous aerosols are considered (Figure 3b). Maximum reduction of anthropogenic AOD (~0.05) occurs over the IGB in the mitigation scenario (Figure 3c) with an area averaged value of 0.018 over India. On the other hand, the anthropogenic AOD increases across India in the mitigation scenario when sulfate aerosols are considered. Specifically, larger increases of anthropogenic AOD (~0.05–0.08) are simulated over the IGB, eastern parts of India and parts of southern India, with an overall increase of ~0.03 when averaged over India (Figure 3f). Apart from the Indian landmass, an increase in anthropogenic AOD (>0.06) is also seen over the northern Bay of Bengal. The regions of increases in anthropogenic AOD over the IGB and eastern coasts of India are consistent with the location of large numbers of high megawatts coal-fired thermal power plants, which emit large amounts of sulfates (Guttikunda & Jawahar, 2014).

The vertical distribution of aerosol extinction in the different experiments is shown in Figure 4. The model simulates the highest concentration of lower tropospheric carbonaceous aerosols in the baseline scenario, with this concentration being substantially reduced in the mitigation scenario (Figures 4a and 4b). The aerosol loadings increase (note the scale of change) in the mitigation scenario when sulfates are included

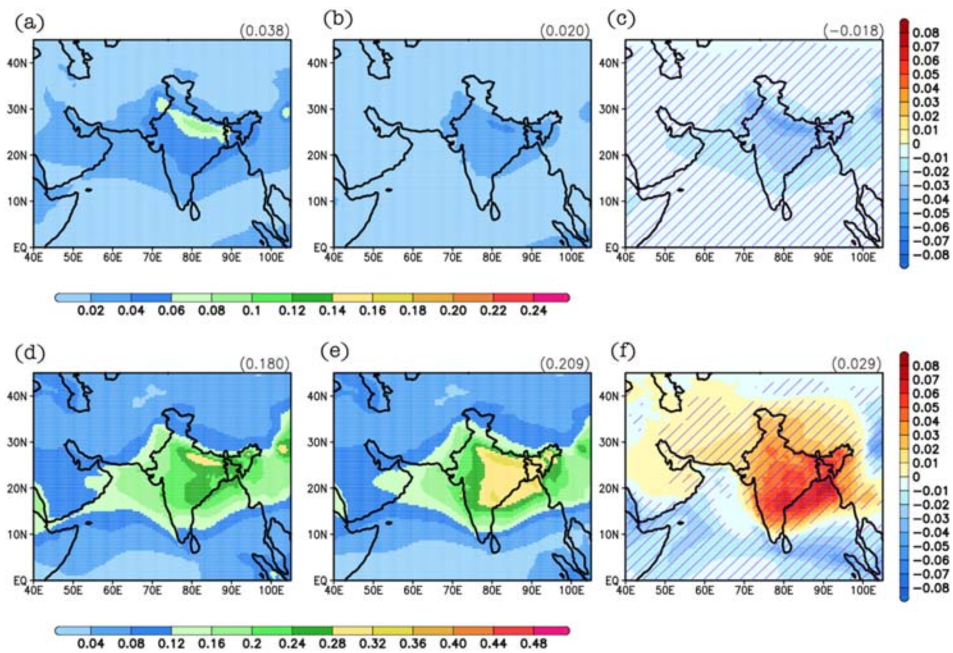

Figure 3. Spatial distribution of mean anthropogenic aerosol optical depth derived from Carb experiments in the top panel: (a) Carb_BS, (b) Carb_MT, and (c) difference between Carb_MT and Carb_BS. Similar arrangements for Suca experiments in the bottom panel: (d) Suca_BS, (e) Suca_MT, and (f) difference between Suca_MT and Suca_BS during the summer monsoon seasons of the period 2006–2015. The oblique violet color lines represent regions with 95% significance. The numbers in the right top corner of each figure are the mean value of AOD over India.

(Figure 4d). In addition, substantial amounts of aerosols are transported from the lower atmosphere to the middle ~600–500 hPa and upper troposphere ~200–100 hPa in all cases. In fact, recent studies (e.g., Lau et al., 2018) have shown that the vertical transport of aerosols can reach the upper troposphere and lower stratosphere, especially during the ISM. This vertical transport is associated with monsoon convective updrafts (as shown Figure 4) and orographic uplift (Fadnavis et al., 2013). Once the aerosols are transported into the upper troposphere, the monsoon easterlies at 200 hPa enhance their horizontal dispersal (Lau et al., 2018). Figure 4 also shows that the quantity of aerosol transported vertically varies depending upon the aerosol loadings in the different scenarios. Finally, the spatial and vertical distributions of aerosols in the baseline and mitigation scenarios imply that the reduction of carbonaceous AOD in the mitigation scenario is overcompensated by an increase in sulfate aerosol emissions.

The mean TOA anthropogenic aerosol-induced radiative forcing for the Carb_BS experiment shows warming (>1.8 W/m^2) over the Thar Desert and Middle East deserts along with the snow-covered regions in the Western Himalayas (Figure 5a). Desert and snow-covered regions reflect more solar radiation due to high albedo causing more interaction with the aerosol layer aloft, and thus enhancing the TOA forcing. The warming at the TOA decreases in the Carb_MT (Figure 5b) by ~0.8–1.4 W/m^2 over the desert- and snow-covered regions, as the BC concentration decreases (Figure 5c). Reduction in TOA warming (~0.2–0.6 W/m^2) is also seen over the IGB for the mitigation scenario. On the other hand, the TOA forcing switches to cooling over central India and the IGB (<−6 W/m^2) when sulfate is considered (Figure 5d). The TOA cooling is more pronounced (<−10 W/m^2) in the case of Suca_MT, especially over the IGB, central and eastern parts of India (Figure 5e), where there is a strong increase in sulfate aerosol loading. The atmospheric radiative forcing obtained from the difference between the radiative forcing at TOA and surface also suggests larger warming (>12 W/m^2) over the IGB and parts of central India in Carb_BS and Suca_BS due to presence of higher BC amounts (Figures S2a and S2d). A slight increase in the atmospheric radiative forcings found especially over the IGB in the Suca experiments compared to Carb experiments could be a result of decreased precipitation and associated washout (as discussed next). Compared to the baseline scenario, the atmospheric radiative forcing is reduced by 2 to 8 W/m^2 over IGB and central India in Carb_MT and Suca_MT, implying greater atmospheric cooling (Figures S2c and S2f).

10.1029/2019JD031414

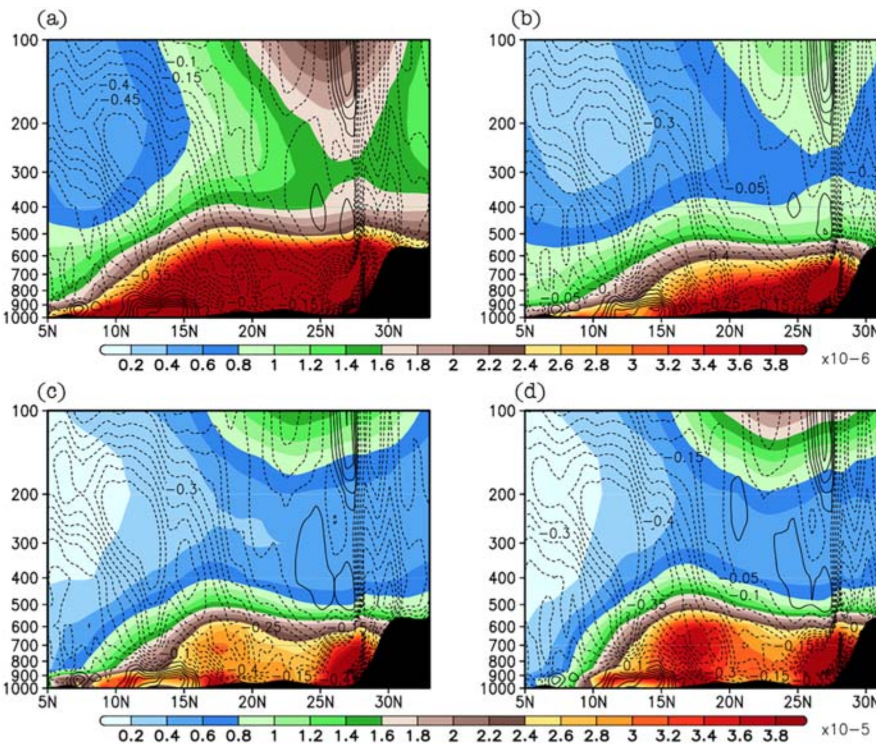

Figure 4. Vertical distribution (averaged over 75–85°E longitudes) of mean anthropogenic aerosol extinction (m^{-1}) and associated vertical pressure velocity ($\times 10^{-4}$ hPa/s) simulated from (a) Carb_BS, (b) Carb_MT, (c) Suca_BS, and (d) Suca_MT experiments during the summer monsoon seasons of the period 2006–2015.

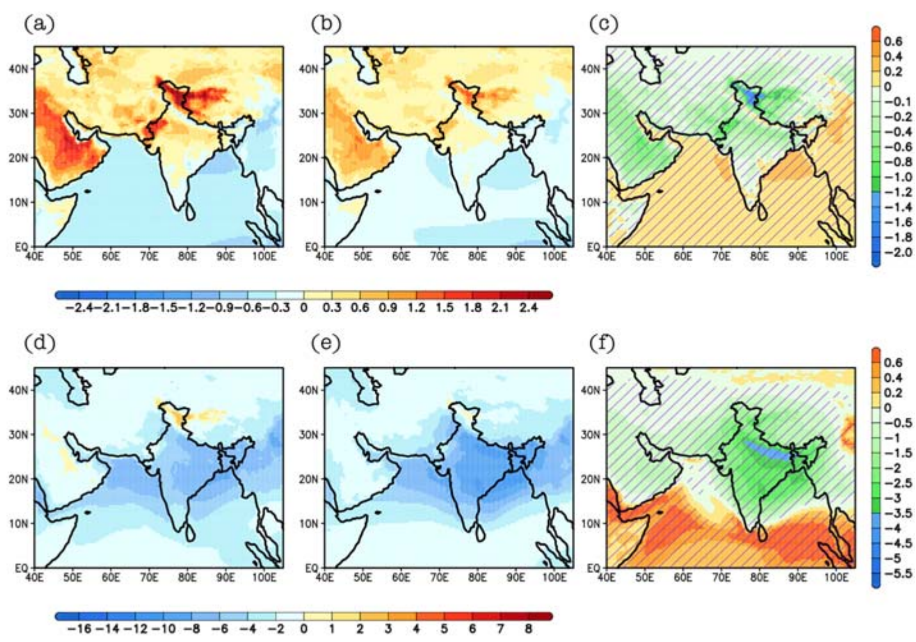

Figure 5. Spatial distribution of mean radiative forcing (W/m^2) at top-of-atmosphere derived from Carb experiments in the top panel: (a) Carb_BS, (b) Carb_MT, and (c) difference between Carb_MT and Carb_BS. Similar arrangements for Suca experiments in the bottom panel: (d) Suca_BS, (e) Suca_MT, and (f) difference between Suca_MT and Suca_BS during the summer monsoon seasons of the period 2006–2015. The oblique violet color lines represent regions with 95% significance.

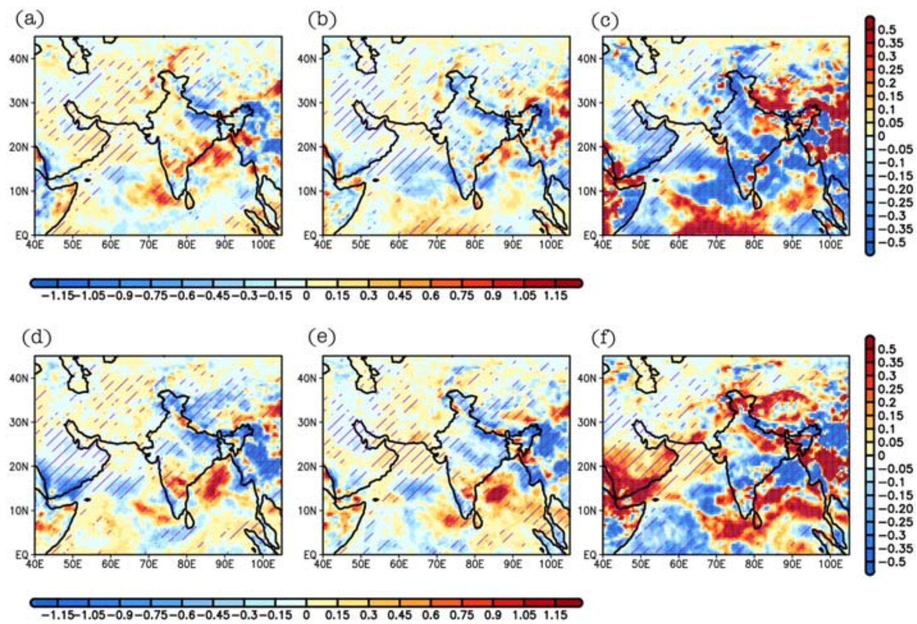

Figure 6. Spatial distribution of anthropogenic aerosol induced changes in mean precipitation (mm/day) simulated from Carb experiments in the top panel: (a) Carb_BS, (b) Carb_MT with respect to Total_CTL, and (c) difference between Carb_MT and Carb_BS. Similar arrangements for Suca experiments in the bottom panel: (d) Suca_BS, (e) Suca_MT with respect to Total_CTL, and (f) difference between Suca_MT and Suca_BS during the summer monsoon seasons of the period 2006–2015. The oblique violet color lines represent regions with 80% significance.

The changes in summer monsoon precipitation induced by the anthropogenic aerosol feedback in the different sensitivity experiments with respect to the Total_CTL, along with the differences between the mitigation and baseline scenarios, are shown in Figure 6. The precipitation responses to these emission scenarios are more evident over the Indian landmass and over the Arabian Sea and Bay of Bengal. Differences with respect to Total_CTL suggest a greater reduction in precipitation (> 0.6 mm/day) over parts of the IGB, central and northeastern India when the sulfate aerosols are included (Figures 6d and 6e) than when only carbonaceous aerosols (Figures 6a and 6b) are considered. Wang et al. (2015) using the CESM global model found a suppression of precipitation due to high amounts of anthropogenic aerosols over Asia. Similar weakening responses in ISM precipitation due to anthropogenic aerosols over South Asia were reported previously using CESM by Ganguly et al. (2012b).

The precipitation response in the Carb_MT and Carb_BS cases shows a decrease in precipitation (~0.1–0.5 mm/day) over most of the Indian continent, the Arabian Sea and the Bay of Bengal in the mitigation scenario in response to a significant decrease in BC-induced atmospheric warming. It is interesting to note that due to presence of more BC-induced atmospheric heating, a small increase in precipitation (~0.15–0.3 mm/day) is simulated over the central and eastern parts of India, and northern Bay of Bengal in Carb_BS (Figure 6a), while precipitation decreases in Carb_MT and Suca_MT. Using the CAM global model, Kovilakam and Mahajan (2016) showed that the ISM precipitation increases linearly with the increases in BC loading. They found that increasing BC emissions simultaneously could enhance moisture transport from the Arabian Sea toward the Indian land areas. The increase in precipitation over the northern Bay of Bengal could be also due to an increase in moisture convergence, which leads to more convective precipitation there (Das et al., 2016).

Comparison of Suca_MT and Suca_BS responses also shows an overall decrease in precipitation, though relatively smaller in magnitude than when only carbonaceous aerosols (Carb_MT-Carb_BS) are considered. Importantly, in both cases the effect of the sulfate induced cooling overwhelms that of BC-induced heating. However, the larger cooling induced by increasing concentrations of sulfates in the Suca_MT contributes to amplify the decrease in precipitation over the central and eastern part of India.

In terms of dynamical responses, the transport of moisture from the Arabian Sea (Figure 7e) is largely inhibited by the aerosol-induced dimming over the Indian landmass due to the overall increase in anthropogenic

10.1029/2019JD031414

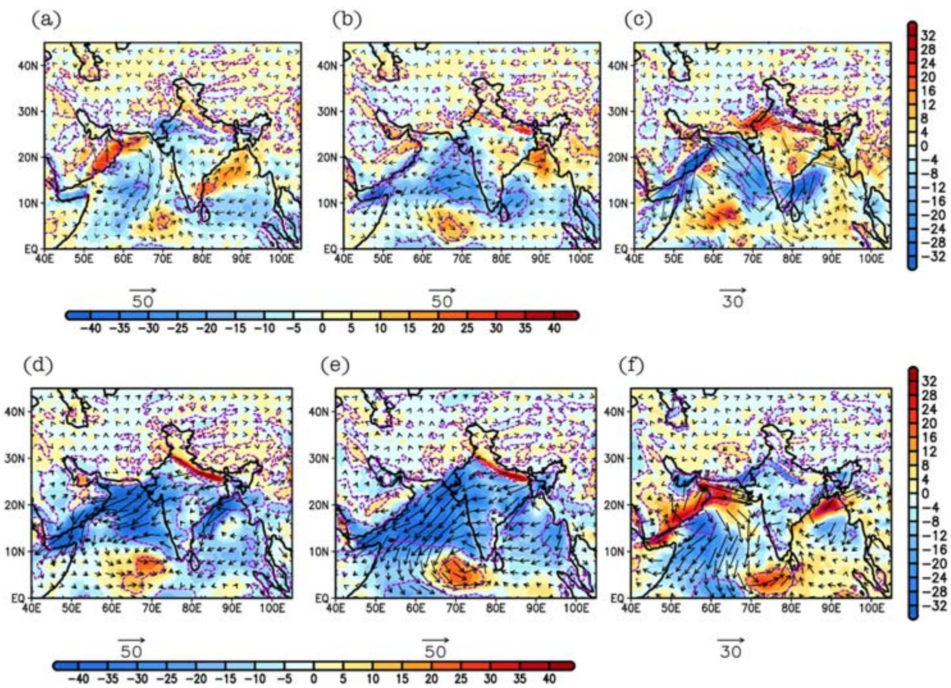

Figure 7. Spatial distribution of anthropogenic aerosol induced changes in the vertical integrated (1,000 to 500 hPa) moisture transport ($kg{\cdot}m^{-1}{\cdot}s^{-1}$) simulated from Carb experiments in the top panel: (a) Carb_BS, (b) Carb_MT with respect to Total_CTL, and (c) difference between Carb_MT and Carb_BS. Similar arrangements for Suca experiments in the bottom panel: (d) Suca_BS, (e) Suca_MT with respect to Total_CTL, and (f) difference between Suca_MT and Suca_BS during the summer monsoon seasons of the period 2006–2015. The oblique violet color lines represent regions with 80% significance.

AOD in Suca_MT. This is also supported by the changes in low-level jet at 850 hPa (Figure S3e), which suggests a maximum decrease in wind magnitude (> 0.5 m/s) over the Arabian Sea and India caused by the anthropogenic aerosol forcing (as also reported in Wang et al., 2015).

The vertical distributions of aerosol-induced changes in air temperature for each case with respect to Total_CTL are shown in Figure 8. BC induces a warming of ~ 0.03–0.09 °C at ~700 to 300 hPa over the central latitudinal bands (10–25°N) in Carb_BS (Figure 8a). At the same time, cooling below 800 hPa is found in response to the aerosol induced low level dimming and the changes in cloud vertical distribution (Figure 9a). Consistently, less pronounced warming occurs in the Carb_MT due to lower amounts of carbonaceous aerosols (Figure 8b). The magnitude of warming in the middle troposphere is reduced when sulfates are included, and in fact a cooling of ~0.15° to 0.24 ° C is seen in the lower troposphere when sulfate aerosols are included (Suca_BS and Suca_MT compared to Carb_BS and Carb_MT) over the latitudinal band 10–25° N. In particular, maximum cooling in the middle and upper troposphere is seen in Suca_MT, along with reduced moisture transport due to weaker winds, which in turn decreases cloud formation over central and eastern India (Figure 9d). This may be attributed to an aerosol-induced reduction of the land-ocean temperature gradient, which weakens the monsoon flow. We also find a temperature increase at 100 hPa, which is associated with aerosol vertical transport at northern latitudes (25–35°N, as discussed in Figure 4). The results show consistent changes in the heating and cooling depending upon the experiment designs. For example, more vertical transport of BC to the upper troposphere in the baseline experiments (Carb_BS and Suca_BS) are related to greater warming (>0.15 °C). Finally, when the high amounts of sulfates are considered (Suca_MT), cooling dominates. The redistribution of aerosol species in the vertical could be important in modulating the thermodynamical structure of the atmosphere (Wang et al., 2015).

In summary, it is clear that the type and magnitude of anthropogenic aerosol species can have different impacts on the monsoon dynamics. For example, the presence of high amounts of BC induces atmospheric heating, which drives relatively stronger monsoon flow and increased moisture flux from the sea, leading to increased rainfall over land. This effect is reversed by the presence of increased sulfate concentrations,

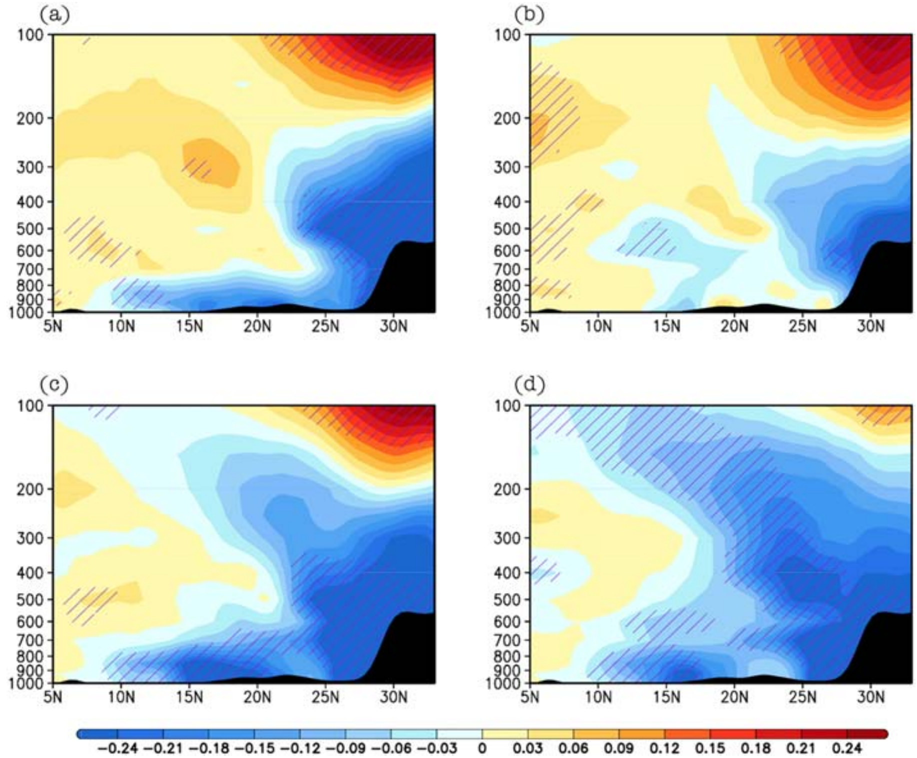

Figure 8. Latitudinal variation of anthropogenic aerosol induced changes in vertical cross sections (averaged over 75–85°E) of air temperature (°C) from (a) Carb_BS, (b) Carb_MT, (c) Suca_BS, and (d) Suca_MT with respect to Total_CTL experiment during the summer monsoon (June–September) seasons of the period 2006–2015. The oblique violet color lines represent regions with 80% significance.

whose cooling effect dominates over the BC heating. In the next section we investigate the interactions of these anthropogenic aerosols in relation to those of aerosols of natural origin.

3.3. Total Aerosol Effects on the ISM Dynamics Under Anthropogenic Aerosol Emission Scenarios

The simulated total AOD for natural (dust and sea salt) and anthropogenic aerosols (Figures 10a and 10b) shows that the total AOD is expected to increase in the mitigation scenario relative to the baseline scenario by >0.04 over India, primarily due to larger amounts of anthropogenic sulfate (>10 mg/m). Manoj et al. (2019) recently showed decreasing trends in BC but increases in total AOD using a dense network of aerosol observatories established under the Aerosol Radiative Forcing over India (ARFINET). Increasing trends in total AOD over some Indian regions were also reported using ARFINET data earlier by Babu et al. (2013).

The atmospheric radiative forcing indicates lower warming over the Indian landmass in the Total_MT compared to Total_BS due to increased emissions of scattering aerosols (Figure 10f). Interestingly, the dust burden is reduced in Total_MT over the Arabian Peninsula and the Arabian Sea, suggesting reduced dust transport toward India (Figure 11d). The decrease in dust loading over the Arabian Sea also contributes to cooling in the mitigation scenario (Figure 10f). Also, the generation of sea-salt and transport over the Arabian Sea is reduced in Total_MT (Figure 11e). One point to note is that the dust burden increases over central India when aerosols are present due to the anthropogenic aerosol-induced decrease in precipitation and washout. This is important, as it implies that changes in the anthropogenic aerosol feedback over India can affect the natural aerosol variability in space and time.

Figure 12a shows an increase in precipitation (~0.6–1.5 mm/day) over the Indian landmass, especially over the west to central parts of India in Total_BS due to enhanced moisture flux from the Arabian Sea (Figure 12b). Therefore, we find that the inclusion of natural aerosols tends to mitigate the dry bias in the Total_CTL. An increase in precipitation (>1.8 mm/day) due to natural aerosols is also simulated over the eastern Arabian Sea and northern Bay of Bengal. Compared to Total_BS, the increase in precipitation is generally lower in Total_MT due to lower moisture transport (Figures 12b and 12e). This can be verified by

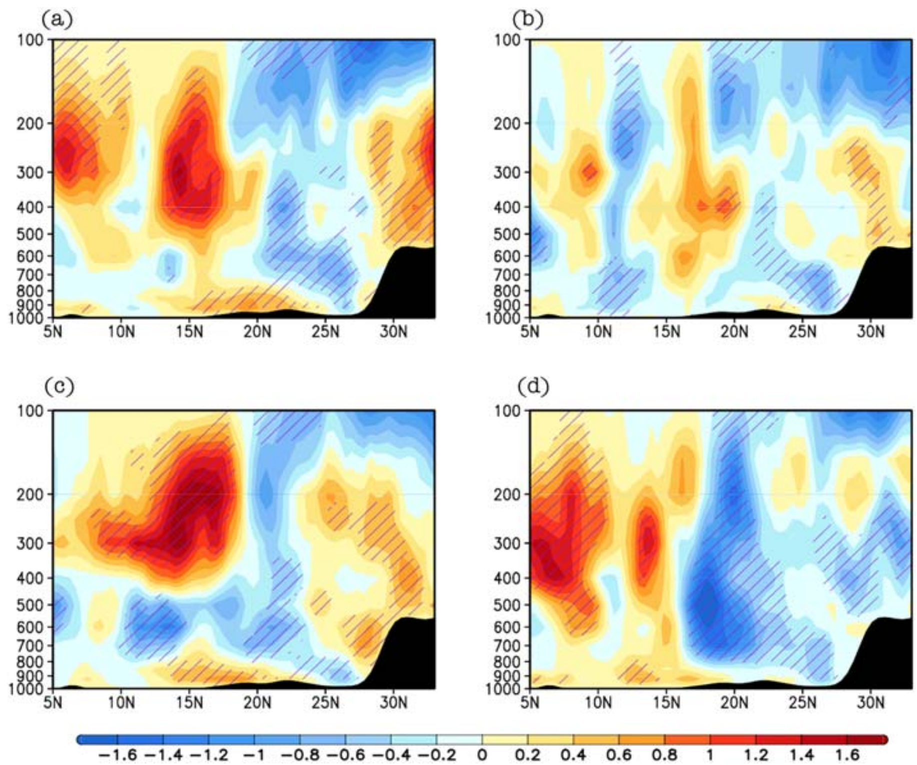

Figure 9. Latitudinal variation of anthropogenic aerosol induced changes in vertical cross sections (averaged over 75–85° E) of cloud fraction ($\times 10^{-2}$ unitless) from (a) Carb_BS, (b) Carb_MT, (c) Suca_BS, and (d) Suca_MT with respect to Total_CTL experiment during the summer monsoon (June–September) seasons of the period 2006–2015. The oblique violet color lines represent regions with 80% significance.

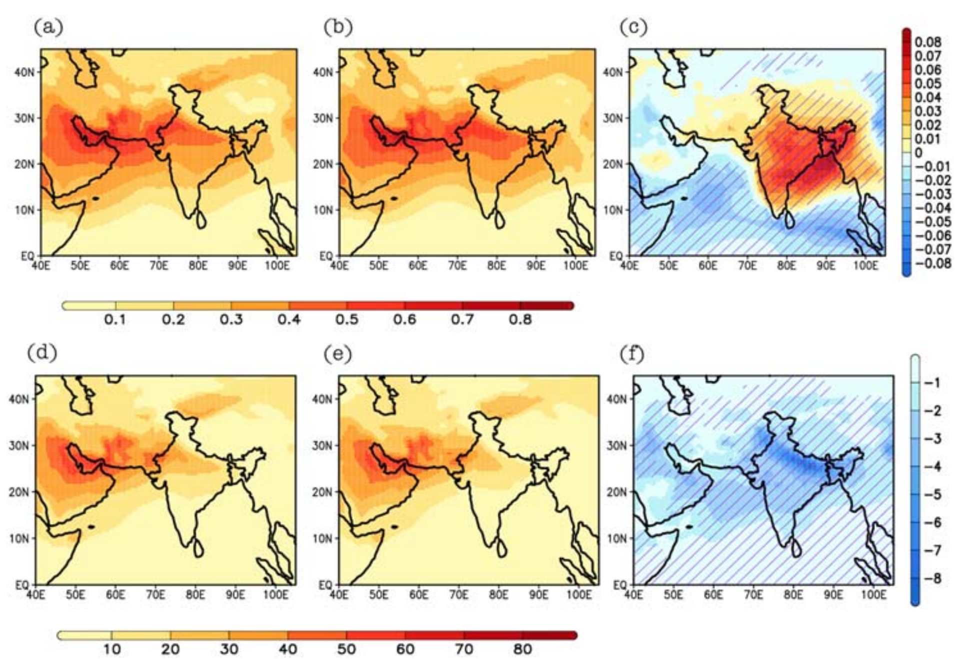

Figure 10. Spatial distribution of mean total aerosol optical depth (top row) and atmospheric radiative forcing (bottom row units: W/m^2) simulated from (a, d) Total_BS (b, e) Total_MT, and (c, f) difference between Total_MT and Total_BS during the summer monsoon (June–September) seasons of the period 2006–2015. The oblique violet color lines in Figures 10c and 10f represent regions with 95% significance.

10.1029/2019JD031414

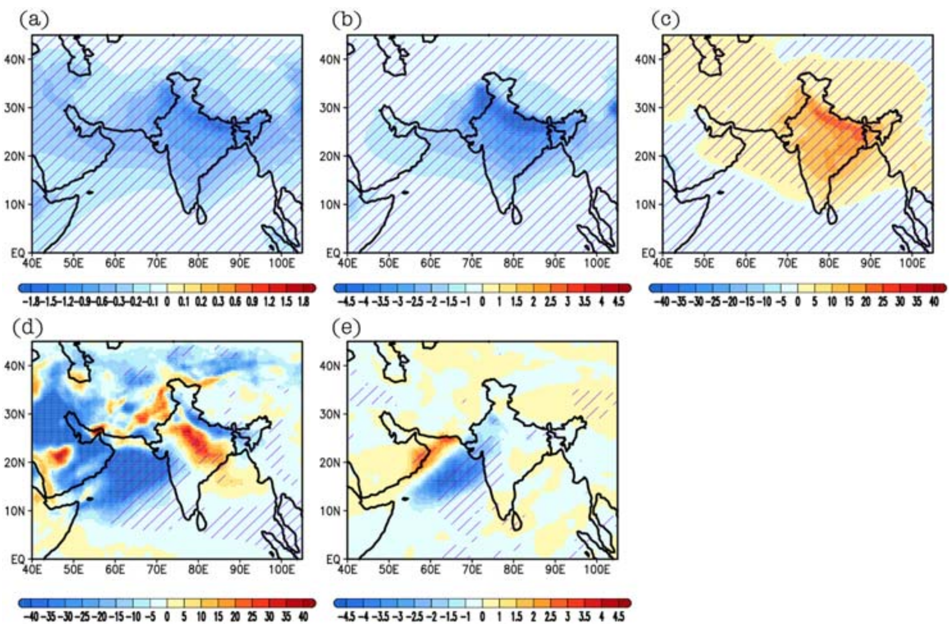

Figure 11. Spatial distribution of changes in mean columnar burden (mg/m^2) for each of the species (a) BC, (b) OC, (c) sulfate, (d) dust, and (e) sea salt obtained from the difference between Total_MT and Total_BS experiments during the summer monsoon (June–September) seasons of the period 2006–2015. The oblique violet color lines represent regions with 90% significance.

looking into the difference in precipitation and moisture between the Total_MT and Total_BS (Figures 12g and 12h). In fact, the decrease in moisture flux of ~30 to 35 kg·m^{-2}·s^{-1} is colocated with the regions of precipitation decrease over the central India, Arabian Sea and northern Bay of Bengal regions in the

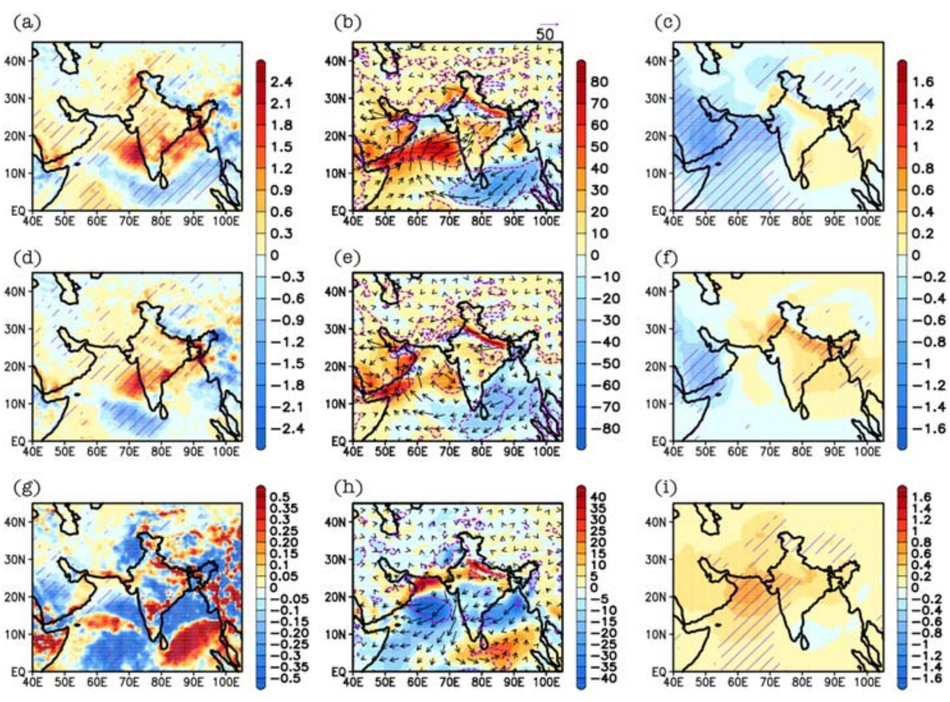

Figure 12. Spatial distribution of total aerosol induced changes in mean precipitation (first column units: mm/day) and vertical moisture transport (second column units: kg·m^{-2}·s^{-1}) and surface pressure (third column units: hPa) simulated from (a–c) Total_BS, (d–f) Total_MT with respect to Total_CTL, and (g–i) difference between Total_MT and Total_BS experiments during the summer monsoon (June–September) seasons of the period 2006–2015. The violet color lines and dashed contours in the plots represent regions with 90% significance.

10.1029/2019JD031414

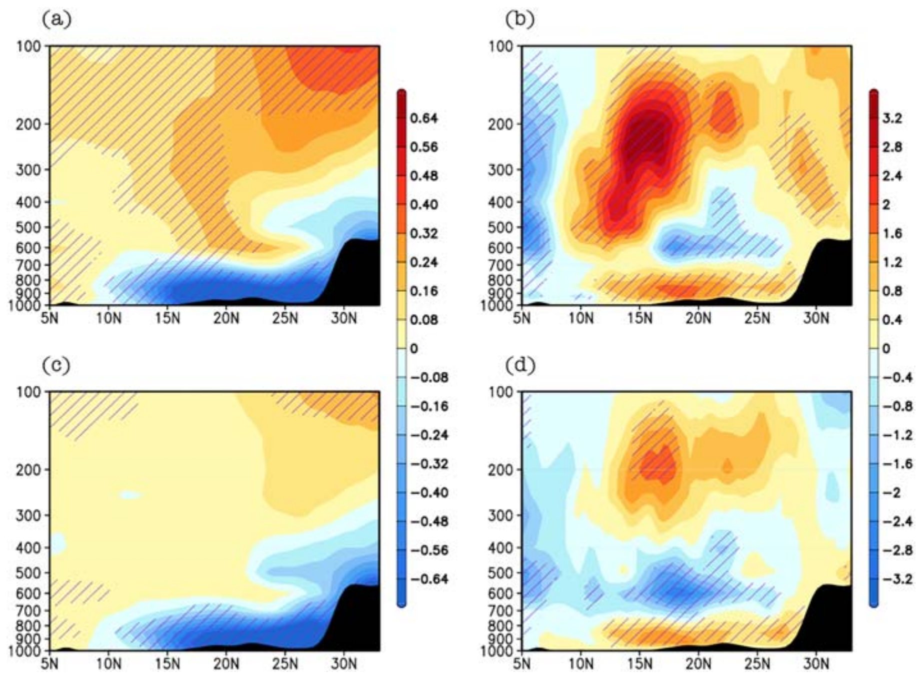

Figure 13. Latitudinal variation of total aerosol induced changes in vertical cross sections (averaged over 75–85° E) of air temperature (°C) and cloud fraction ($\times 10^{-2}$) from (a and b) Total_BS and (c and d) Total_MT with respect to Total_CTL experiment respectively during the summer monsoon (June–September) seasons of the period 2006–2015. The oblique violet color lines represent regions with 90% significance.

mitigation scenario. The increase in moisture flux in the Total_BS (Figure 12b) could be related to the strengthening of the wind circulations (at 850 hPa) due to large-scale convergence of the monsoon winds with the Shamal winds in Saudi Arabia and the northerly Lever winds coming from Iran over the Arabian Peninsula. Our results are consistent with recent studies carried out by Vinoj et al. (2014), Jin et al. (2014), Das, Dey, Dash, Giuliani, et al. (2015), which suggested the existence of a positive feedback between the Middle East desert dust aerosols and the ISM. More intensified winds (>1 m/s) in Total_BS compared to the Total_CTL (Figure S4) are simulated over the Arabian Sea, southern part of the Indian continent and the northern Bay of Bengal because of a reduction in the mean surface air pressure over the Arabian Peninsula (Figure 12c) associated with dust induced large-scale tropospheric warming (Vinoj et al., 2014). Thus, our results indicate that the anthropogenic aerosols tend to decrease the monsoon precipitation over the Indian subcontinent whereas the inclusion of natural aerosols (particularly dust) can compensate this loss.

The changes in air temperature vertical profile over the Indian subcontinent show heating of the middle and upper troposphere in the Total_BS case (Figure 13a), which gradually decreases in Total_MT case (Figure 13c) due to atmospheric cooling caused by increasing concentrations of sulfate aerosols. The increase in the middle and upper tropospheric temperature causes enhanced moisture transport from the Arabian Sea, and consequently precipitation, in Total_BS compared to Total_MT as seen in Figure 12. Higher magnitude of warming (~0.16–0.4 °C) is found in the lower to upper troposphere when dust is considered in the Total_BS compared to Carb_BS.

In Total_BS, the precipitation increase over central India can also be associated with the joint response of the local boundary layer over the region and the stronger monsoon wind providing additional moisture. Due to a stronger wind, more moisture is transported over central India and the simultaneous stabilization of the lower troposphere caused by dimming facilitates cloud and fog formation (Figure 13b). The increased low-level cloudiness is more pronounced within the latitudinal band 15–25°N in Total_BS compared to Total_MT and is due to an aerosol-induced “capping effect,” which prevents moisture transport to the upper troposphere. A similar response was seen in a study of dust aerosol impacts on the African monsoon system by Solmon et al. (2012). A smaller increase in low-level clouds over central India occurs in Total_MT (Figure 13d) due to lower moisture availability over the region. South of 15°N, and especially between

10°N and 15°N, there are lower amounts of high clouds in Total_MT because of reduced convective activity occurring in response to the weakening of the monsoon winds compared to Total_BS (Figure S4c).

4. Summary and Conclusions

In this study we examined the dynamical response of the ISM to anthropogenic aerosol emission scenarios (baseline vs. mitigation) taken from the ECLIPSE inventory using the RCM RegCM4 coupled with an online aerosol module. We conducted a series of 11-year long sensitivity experiments designed to isolate anthropogenic aerosol impacts under a near term mitigation scenario (where BC and OC are projected to decrease and sulfate to increase) relative to a baseline scenario, without considering changes in climate induced by increases in GHG concentrations.

The main conclusions of our study can be summarized as follows:

1. The increase in sulfate aerosols in the mitigation scenario is expected to overcompensate the reduction in carbonaceous aerosols, leading to an increase in anthropogenic AOD over the ISM region.
2. The ISM is sensitive to anthropogenic aerosol feedbacks both in its spatial and temporal characteristics. Larger reductions in wind circulation and precipitation are expected in the mitigation scenario relative to the baseline scenario because of a weakening of the land-sea thermal heating gradient caused by enhanced atmospheric cooling over the Indian landmass due to larger sulfate loadings.
3. If natural aerosols are included in the simulation, the impact of dust feedback becomes an important factor. The ISM strengthens in response to the strengthening of moisture carrying winds due to large-scale convergence of winds over the Arabian Peninsula. However, the increase in precipitation is lower in the mitigation than the baseline scenario due to the weakening of moisture carrying winds from the Arabian Sea.
4. The space-time variability of natural aerosols is modulated by the anthropogenic aerosol feedback. The decrease in wind circulation in the mitigation scenario causes lower dust transport across the Arabian Sea from the Arabian Peninsula. This reduces precipitation over central India and parts of the eastern Arabian Sea and northern Bay of Bengal.

Our study should be interpreted in view of the following limitations. First, the model does not consider the indirect effects of aerosols (Albrecht, 1989). Recent studies (e.g., Sarangi et al., 2018) have suggested that aerosols might favor monsoon cloud formation over India through the process of invigoration. An increase in sulfates over India could thus facilitate more cloud formation. Second, the model is not coupled to an ocean model and therefore does not consider possible aerosol induced SST feedbacks. However, SST responses to aerosol dimming are slow and would be most effective in a longer climatic scale (Ganguly et al., 2012a). Third, in order to isolate the effects of aerosols we used the same present-day meteorological boundary conditions in all sensitivity experiments. However, it would be useful to investigate aerosol effects within the context of GHG-induced changes in regional circulations and climate. For example, Zhao et al. (2019) suggest that aerosol mitigation could induce stronger responses in extreme precipitation under the high end RCP85 GHG concentration scenario. Fourth, our model assumes only external aerosol mixing. The internal mixing of different aerosol species, for example, BC coated by sulfates can enhance the atmospheric heating. In fact, Dey et al. (2008) suggested that internal mixing between the aerosol species over the IGB could modulate the absorptive properties of the composite aerosol. Fifth, in our model we do not include all anthropogenic aerosols (e.g., secondary OC and brown carbon), which could indeed modulate the responses and are worth implementing in the aerosol module. Finally, the internal variability of the model could potentially induce some noise, but given the length of our simulations, we believe that the climate signals detected are consistent in many respects with the available literature. An ensemble approach with perturbed boundary conditions may be a possible way to reduce the effect of the model's internal variability but requires heavy computation resources. All these issues will be addressed in future work.

Notwithstanding these limitations, our study confirms that the emission of atmospheric aerosols of anthropogenic origin can affect the ISM and that this effect is substantially modulated by the presence of natural aerosols. It also shows that the chemical and physical characteristics of the aerosols are critical in determining the aerosol effects on the ISM, and that both natural and anthropogenic aerosols need to be considered in studies of climate-aerosol interactions over the region. We find that the mitigation scenario derived from the ECLIPSE project is not sufficient to ameliorate the aerosol impacts on the ISM, and indeed this scenario decreases the ISM intensity mostly due to an increase in the atmospheric sulfate burden. This can have significant impacts on the hydrologic cycle of the region and, along with the health risk induced by high levels of atmospheric pollution, calls for more stringent mitigation measures, especially for sulfates. Though more studies with other climate models and better emission inventories are required to assess the robustness of our results, we can certainly conclude that the ISM response to aerosol radiative feedbacks needs to be considered when designing emission scenarios to combat air pollution and climate change over India.

Acknowledgments
The authors are thankful to supercomputing facility provided by Marconi installed in CINECA machine, where all the simulations were carried out. The model RegCM4 code is freely available online (from http://gforge.ictp.it/gf/project/regcm/). The anthropogenic aerosol emissions considered for baseline and mitigation of SLCPs are taken from ECLIPSE data inventory. The data used can be easily accessed online (http://www.iiasa.ac.at/web/home/research/researchPrograms/air/ECLIPSEv5a.html). Both GPCP and MISR observed precipitation and AOD data can be assessed from https://giovanni.gsfc.nasa.gov/giovanni/ website. The AERONET data can be assessed from https://aeronet.gsfc.nasa.gov/cgi-bin/webtool_aod_v3 website. All the PIs of AERONET stations data used in our study are highly acknowledged. Both data and input files for RegCM4 model are archived in http://clima-dods.ictp.it/regcm4/ website. S. Dey acknowledges support from IIT Delhi for the Institute Chair. The authors would like to thank anonymous reviewers for their comments that helped improving the quality of the manuscript.

References

Albrecht, B. A. (1989). Aerosols, cloud microphysics, and fractional cloudiness. *Science*, *245*(4923), 1227–1230. https://doi.org/10.1126/science.245.4923.1227

Babu, S. S., Manoj, M. R., Moorthy, K. K., Gogo, M. M., Nair, V. S., Kompalli, S. K., et al. (2013). Trends in aerosol optical depth over Indian region: Potential causes and impact indicators. *Journal of Geophysical Research: Atmospheres*, *118*, 11,794–11,806. https://doi.org/10.1002/2013JD020507

Baker, L. H., Collins, W. J., Olivié, D. J. L., Cherian, R., Hodnebrog, Ø., Myhre, G., & Quaas, J. (2015). Climate responses to anthropogenic emissions of short-lived. *Atmospheric Chemistry and Physics*, *15*(14), 8201–8216. https://doi.org/10.5194/acp-15-8201-2015

Bollasina, M., Ming, Y., & Ramaswamy, V. (2011). Anthropogenic aerosols and the weakening of the South Asian summer monsoon. *Science*, *334*(6055), 502–505. https://doi.org/10.1126/science.1204994

Bond, T. C., Doherty, S. J., Fahey, D. W., Forster, P. M., Berntsen, T., Deangelo, B. J., et al. (2013). Bounding the role of black carbon in the climate system: A scientific assessment. *Journal of Geophysical Research: Atmospheres*, *118*(11), 5380–5552. https://doi.org/10.1002/jgrd.50171

Chakraborty, A., Gupta, T., & Tripathi, S. N. (2016). Chemical composition and characteristics of ambient aerosols and rainwater residues during Indian summer monsoon: Insight from aerosol mass spectrometry. *Atmospheric Environment*, *136*, 144–155.

Cohen, A. J., Brauer, M., Burnett, R., Anderson, H. R., Frostad, J., Estep, K., et al. (2017). Estimates and 25-year trends of the global burden of disease attributable to ambient air pollution: An analysis of data from the Global Burden of Diseases Study 2015. *The Lancet*, *389*(10082), 1907–1918. https://doi.org/10.1016/S0140-6736(17)30505-6

Das, S., Dey, S., & Dash, S. K. (2015). Impacts of aerosols on dynamics of Indian summer monsoon using a regional climate model. *Climate Dynamics*, *44*(5-6), 1685–1697. https://doi.org/10.1007/s00382-014-2284-4

Das, S., Dey, S., & Dash, S. K. (2016). Direct radiative effects of anthropogenic aerosols on Indian summer monsoon circulation. *Theoretical and Applied Climatology*, *124*(3-4), 629–639. https://doi.org/10.1007/s00704-015-1444-8

Das, S., Dey, S., Dash, S. K., & Basil, G. (2013). Examining mineral dust transport over the Indian subcontinent using the regional climate model, RegCM4.1. *Atmospheric Research*, *134*, 64–76. https://doi.org/10.1016/j.atmosres.2013.07.019

Das, S., Dey, S., Dash, S. K., Giuliani, G., & Solmon, F. (2015). Dust aerosol feedback on the Indian summer monsoon: Sensitivity to absorption property. *Journal of Geophysical Research: Atmospheres*, *120*, 9642–9652. https://doi.org/10.1002/2015JD023589

Dash, S. K., Mamgain, A., Pattnayak, K. C., & Giorgi, F. (2013). Spatial and temporal variations in Indian summer monsoon rainfall and temperature: An analysis based on RegCM3 simulations. *Pure and Applied Geophysics*, *170*(4), 655–674. https://doi.org/10.1007/s00024-012-0567-4

Dash, S. K., Shekhar, M. S., & Singh, G. P. (2006). Simulation of Indian summer monsoon circulation and rainfall using RegCM3. *Theoretical and Applied Climatology*, *86*(1-4), 161–172. https://doi.org/10.1007/s00704-006-0204-1

Dee, D. P., Uppala, S. M., Simmons, A. J., Berrisford, P., Poli, P., Kobayashi, S., et al. (2011). The ERA-Interim reanalysis: Configuration and performance of the data assimilation system. *Quarterly Journal of the Royal Meteorological Society*, *137*, 553–597. https://doi.org/10.1002/qj.828

Dey, S., & Di Girolamo, L. (2010). A climatology of aerosol optical and microphysical properties over the Indian subcontinent from 9 years (2000–2008) of Multiangle Imaging Spectroradiometer (MISR) data. *Journal of Geophysical Research*, *115*, D15204. https://doi.org/10.1029/2009JD013395

Dey, S., & Di Girolamo, L. (2011). A decade of change in aerosol properties over the Indian subcontinent. *Geophysical Research Letters*, *38*, L14811. https://doi.org/10.1029/2011GL048153

Dey, S., Tripathi, S. N., & Mishra, S. K. (2008). Probable mixing state of aerosols in the Indo-Gangetic Basin, northern India. *Geophysical Research Letters*, *35*, L03808. https://doi.org/10.1029/2007GL032622

Dubovik, O., Holben, B., Eck, T. F., Smirnov, A., Kaufman, Y. J., King, M. D., et al. (2002). Variability of absorption and optical properties of key aerosol types observed in worldwide locations. *Journal of Atmospheric Science*, *59*(3), 590–608.

Emanuel, K., & Zivkovic, R. M. (1999). Development and evaluation of a convection scheme for use in climate models. *Journal of the Atmospheric Sciences*, *56*1766–1782.

Fadnavis, S., Semeniuk, K., Pozzoli, L., Schultz, M. G., Ghude, S. D., Das, S., & Kakatkar, R. (2013). Transport of aerosols into the UTLS and their impact on the Asian monsoon region as seen in a global model simulation. *Atmospheric Chemistry and Physics*, *13*, 8771–8786. https://doi.org/10.5194/acp-13-8771-2013

Flanner, M. G., Zender, C. S., Randerson, J. T., & Rasch, P. J. (2007). Present-day climate forcing and response from black carbon in snow. *Journal of Geophysical Research*, *112*, D11202. https://doi.org/10.1029/2006JD008003

Gadhavi, H. S., Renuka, K., Kiran, V. R., Jayaraman, A., Stohl, A., Klimont, Z., & Beig, G. (2015). Evaluation of black carbon emission inventories using a Lagrangian dispersion model—A case study over southern India. *Atmospheric Chemistry and Physics*, *15*(3), 1447–1461. https://doi.org/10.5194/acp-15-1447-2015

Ganguly, D., Rasch, P. J., Wang, H., & Yoon, J. (2012a). Fast and slow responses of the South Asian monsoon system to anthropogenic aerosols. *Geophysical Research Letters*, *39*, L18804. https://doi.org/10.1029/2012GL053043

Ganguly, D., Rasch, P. J., Wang, H., & Yoon, J.-H. (2012b). Climate response of the South Asian monsoon system to anthropogenic aerosols. *Journal of Geophysical Research*, *117*, D13209. https://doi.org/10.1029/2012JD017508

Ghosh, S., Bhatla, R., Mall, R. K., Srivastava, P. K., & Sahai, A. K. (2019). Aspect of ECMWF downscaled Regional Climate Modeling in simulating Indian summer monsoon rainfall and dependencies on lateral boundary conditions. *Theoretical and Applied Climatology*, *135*(3-4), 1559–1581. https://doi.org/10.1007/s00704-018-2432-6

Giles, D. M., Sinyuk, A., Sorokin, M. G., Schafer, J. S., Smirnov, A., Slutsker, I., et al. (2019). Advancements in the Aerosol Robotic Network (AERONET) Version 3 database—Automated near-real-time quality control algorithm with improved cloud screening for Sun photometer aerosol optical depth (AOD) measurements. *Atmospheric Measurement Techniques*, *12*(1), 169–209.

Giorgi, F. (2019). Thirty years of regional climate modeling: Where are we and were are we going? *Journal of Geophysical Research*, *124*, 5696–5723.

Giorgi, F., Bi, X., & Qian, Y. (2002). Direct radiative forcing and regional climatic effects of anthropogenic aerosols over East Asia: A regional coupled climate-chemistry/aerosol model study. *Journal of Geophysical Research*, *107*, AAC-7. https://doi.org/10.1029/2001JDOO1066

Giorgi, F., Coppola, E., Solmon, F., Mariotti, L., Sylla, M., Bi, X., et al. (2012). RegCM4: Model description and preliminary tests over multiple CORDEX domains. *Climate Research*, *52*, 7–29. https://doi.org/10.3354/cr01018

Giorgi, F., Jones, C., & Asrar, G. (2009). Addressing climate information needs at the regional level:the CORDEX framework. *WMO Bulletin*, *58*, 175–183.

Grenier, H., & Bretherton, C. S. (2001). A moist PBL parameterization for large-scale models and its application to subtropical cloud-topped marine boundary layers. *Monthly Weather Review*, *129*, 357–377. https://doi.org/10.1175/1520-0493(2001)129<0357:AMPPFL>2.0.CO;2

Guttikunda, S. K., & Jawahar, P. (2014). Atmospheric emissions and pollution from the coal-fired thermal power plants in India. *Atmospheric Environment*, *92*, e11–e11. https://doi.org/10.1016/j.atmosenv.2014.04.057

Haywood, J., & Boucher, O. (2000). Estimates of the direct and indirect radiative forcing due to tropospheric aerosols: A review. *Reviews of Geophysics*, *513–543*.

Huffman, G.J., R.F. Adler, D.T. Bolvin, K. Hsu, C. Kidd, E.J. Nelkin, et al., (2019), Algorithm Theoretical Basis Document (ATBD) for global precipitation climatology project version 3.0 precipitation data. MEaSUREs project, Greenbelt, MD, 26 pp.

Jiang, Y., Liu, X., Yang, X. Q., & Wang, M. (2013). A numerical study of the effect of different aerosol types on East Asian summer clouds and precipitation. *Atmospheric Environment*, *70*, 51–63.

Jiang, Y., Yang, X.-Q., & Liu, X. (2015). Seasonality in anthropogenic aerosol effects on East Asian climate simulated with CAM5. *Journal of Geophysical Research: Atmospheres*, *120*, 10,837–10,861. https://doi.org/10.1002/2015JD023451

Jiang, Y., Yang, X.-Q., Liu, X., Yang, D., Sun, X., Wang, M., et al. (2017). Anthropogenic aerosol effects on East Asian winter monsoon: The role of black carbon-induced Tibetan Plateau warming. *Journal of Geophysical Research: Atmospheres*, *122*, 5883–5902. https://doi.org/10.1002/2016JD026237

Jin, Q., Wei, J., Pu, B., Yang, Z., & Parajuli, S. P. (2018). High summertime aerosol loadings over the Arabian Sea and their transport pathways. *Journal of Geophysical Research: Atmospheres*, *123*(18):10–568. https://doi.org/10.1029/2018JD028588

Jin, Q., Wei, J., & Yang, Z. (2014). Positive response of Indian summer rainfall to Middle East dust, 4068–4074. *Geophysical Research Letters*. *41*, 11 4068–4074 https://doi.org/10.1002/2014GL059980

Jin, Q., Wei, J., Yang, Z. L., Pu, B., & Huang, J. (2015). Consistent response of Indian summer monsoon to Middle East dust in observations and simulations. *Atmospheric Chemistry and Physics Discussions*, *15*(11), 15,571–15,619. https://doi.org/10.5194/acpd-15-15571-2015

Jin, Q., Yang, Z., & Wei, J. (2016). High sensitivity of Indian summer monsoon to Middle East dust absorptive properties. *Scientific Reports*, *6*(1), 1–8. https://doi.org/10.1038/srep30690

Kahn, R. A., Gaitley, B. J., Garay, M. J., Diner, D. J., Eck, T. F., Smirnov, A., & Holben, B. N. (2010). Multiangle Imaging SpectroRadiometer global aerosol product assessment by comparison with the Aerosol Robotic Network. *Journal of Geophysical Research*, *115*. https://doi.org/10.1029/2010JD014601

Kiehl, J. T., J. J. Hack, G. B. Bonan, B. A. Boville, B. P. Breigleb, D. Williamson, and P. Rasch (1996), Description of the NCAR community climate model (CCM3), Tech. Rep. National Center for Atmospheric Research, NCAR/TN-420 + STR.

Kovilakam, M., & Mahajan, S. (2016). Confronting the “Indian summermonsoon response to black carbon aerosol” with the uncertainty in its radiative forcing and beyond. *Journal of Geophysical Research: Atmospheres*, *121*, 7833–7852. https://doi.org/10.1002/2016JD024866

Lau, K. M., & Kim, K. M. (2006). Observational relationships between aerosol and Asian monsoon rainfall, and circulation. *Geophysical Research Letters*, *33*, L21810. https://doi.org/10.1029/2006GL027546

Lau, W. K. M., Yuan, C., & Li, Z. (2018). Origin, maintenance and variability of the Asian Tropopause Aerosol Layer (ATAL): The roles of monsoon dynamics. *Scientific Reports*, *8*(1), 1–14. https://doi.org/10.1038/s41598-018-22267-z

Li, C., Mclinden, C., Fioletov, V., Krotkov, N., Carn, S., Streets, D., et al. (2017). India is overtaking China as the world's largest emitter of anthropogenic sulfur dioxide. *Scientific Reports*, 1–7. https://doi.org/10.1038/s41598-017-14639-8

Lin, G., Penner, J. E., Flanner, M. G., Sillman, S., Xu, L., & Zhou, C. (2014). Radiative forcing of organic aerosol in the atmosphere and on snow: Effects of SOA and brown carbon. *Journal of Geophysical Research: Atmospheres*, *119*, 7453–7476. https://doi.org/10.1002/2013JD021186

Liu, X., Xie, X., Yin, Z.-Y., Liu, C., & Gettelman, A. (2011). A modeling study of the effects of aerosols on clouds and precipitation over East Asia. *Theoretical and Applied Climatology*, *106*(3–4), 343–354. https://doi.org/10.1007/s00704-011-0436-6

Maharana, P., Kumar, D., & Dimri, A. P. (2019). Assessment of coupled regional climate model (RegCM4.6–CLM4.5) for Indian summer monsoon. *Climate Dynamics*, *53*(11), 6543–6558. https://doi.org/10.1007/s00382-019-04947-2

Manoj, M. R., Satheesh, S. K., Moorthy, K. K., Gogoi, M. M., & Babu, S. S. (2019). Decreasing trend in black carbon aerosols over the Indian region. *Geo. Phy Lett.*. https://doi.org/10.1029/2018GL081666

Menon, S., Hansen, J., & Nazarenko, L. (2002). Climate effects of black carbon aerosols in China and India. *Science*, *297*(September), 2250–2254.

Mishra, S. K., Sahany, S., Salunke, P., Kang, I.-S., & Jain, S. (2018). Fidelity of CMIP5 multi model mean in assessing Indian monsoon simulations. *npj Climate and Atmospheric Sciences*, *1*(1), 39. https://doi.org/10.1038/s41612-018-0049-1

Moorthy, K. K., Babu, S. S., Manoj, M. R., & Satheesh, S. K. (2013). Build up of aerosols over the Indian Region. *Geophysical Research Letters*, *40*, 1011–1014. https://doi.org/10.1002/grl.50165

Myhre, G., Stordal, F., Bergelen, T. F., Sundet, J. K., & Isaksen, I. S. A. (2004). Uncertainties in the Radiative Forcing Due to Sulfate Aerosols. *Journal of the Atmospheric Sciences*, *6*(5), 485–498. https://doi.org/10.1175/1520-0469(2004)061<0485:uitrfd>2.0.co;2

Nair, V. S., Solmon, F., Giorgi, F., Mariotti, L., Babu, S. S., & Moorthy, K. K. (2012). Simulation of South Asian aerosols for regional climate studies. *Journal of Geophysical Research: Atmospheres*, *117*(4), 1–17. https://doi.org/10.1029/2011JD016711

Oleson, K. W., Lawrence, D. M., Bonan, G. B., Drewniak, B., Huang, M., Koven, C. D., et al. (2013). Technical description of version 4.5 of the Community Land Model (CLM). NCAR/TN-503 + STR *NCAR Tech Note* 266.

Pal, J. S., Small, E. E., & Eltahir, E. A. B. (2000). Simulation of regional-scale water and energy budgets: Representation of subgrid cloud and precipitation processes within RegCM. *Journal of Geophysical Research: Atmospheres*, *105*, 29,579–29,594. https://doi.org/10.1029/2000JD900415

Qian, Y., Giorgi, F., Huang, Y., Chameides, W., & Luo, C. (2001). Regional simulation of anthropogenic sulfur over East Asia and its sensitivity to model parameters, *Tellus*. *Ser. B Chem. Phys. Meteorol.*, *53*(2), 171–191. https://doi.org/10.1034/j.1600-0889.2001.d01-14.x

Raju, P. V. S., Bhatla, R., Almazroui, M., & Assiri, M. (2015). Performance of convection schemes on the simulation of summer monsoon features over the South Asia CORDEX domain using RegCM-4 *Int. Jour. Clim. DOI*. https://doi.org/10.1002/joc.4317

Ramanathan, V., Chung, C., Kim, D., Bettge, T., Buja, L., Kiehl, J. T., et al. (2005). Atmospheric brown clouds: Impacts on South Asian climate and hydrological cycle. *Proc. Natl. Acad. Sci. United States Am.*, *102*(15), 5326–5333.

Rana, A., Jia, S., & Sarkar, S. (2019). Black carbon aerosol in India: A comprehensive review of current status and future prospects. *Atmospheric Research*, *218*, 207–230.

Sarangi, S., Kanawade, V. P., Tripathi, S. N., Thomas, A., & Ganguly, D. (2018). Aerosol-induced intensification of cooling effect of clouds during Indian summer monsoon. *Nature Communications*, *9*(1), 1–9. https://doi.org/10.1038/s41467-018-06015-5

Shindell, D., Unger, N., Koch, D., Faluvegi, G., Bauer, S., Ammann, M., et al. (2008). Climate forcing and air quality change due to regional emissions reductions by economic sector. *Atmospheric Chemistry and Physics*, 7101–7113.

Singh, S., Ghosh, S., Sahana, A. S., Vittal, H., & Karmakar, S. (2016). Do dynamic regional models add value to the global model projections of Indian monsoon? *Climate Dynamics*, *48*(3-4), 1375–1397. https://doi.org/10.1007/s00382-016-3147-y

Solmon, F., Elguindi, N., & Mallet, M. (2012). Radiative and climatic effects of dust over West Africa, as simulated by a regional climate model. *Climate Research*, *52*, 97–113.

Solmon, F., Giorgi, F., & Liousse, C. (2006). Aerosol modelling for regional climate studies: Application to anthropogenic particles and evaluation over a European/African domain. *Tellus B*, *58*(1), 51–72.

Solmon, F., Nair, V. S., & Mallet, M. (2015). Increasing Arabian dust activity and the Indian summer monsoon. *Atmospheric Chemistry and Physics*, 8051–8064. https://doi.org/10.5194/acp-15-8051-2015

Sperber, K. R., Annamalai, H., Kang, I. S., Kitoh, A., Moise, A., Turner, A., et al. (2013). The Asian summer monsoon: An intercomparison of CMIP5 vs. CMIP3 simulations of the late 20th century. *Climate Dynamics*, *41*(9–10), 2711–2744. https://doi.org/10.1007/s00382-012-1607-6

Stohl, A., Aamaas, B., Amann, M., Baker, L. H., Bellouin, N., Berntsen, T. K., et al. (2015). Evaluating the climate and air quality impacts of short-lived pollutants. *Atmospheric Chemistry and Physics*, *10529–10566*.

Sun, H., & Liu, X. D. (2015). Numerical simulation of the direct radiative effects of dust aerosol on the East Asian Winter Monsoon. *Advances in Meteorology*. https://doi.org/10.1155/2015/142617

Tiedtke, M. (1989). A comprehensive mass flux scheme for cumulus parameterization in large-scale models. *Monthly Weather Review*, *117*, 1779–1800.

Tiwari, S., Mishra, A. K., & Singh, A. K. (2016). Aerosol climatology over the Bay of Bengal and Arabian Sea inferred from space-borne radiometers and lidar observations. *Aerosol and Air Quality Research*, *16*(11), 2855–2868. https://doi.org/10.4209/aaqr.2015.06.0406

Tummon, F., Solmon, F., Liousse, C., & Tadross, M. (2010). Simulation of the direct and semidirect aerosol effects on the southern Africa regional climate during the biomass burning season. *Journal of Geophysical Research: Atmospheres*, *115*(19), 1–20. https://doi.org/10.1029/2009JD013738

Twomey, S. (1974). Pollution and the planetary albedo. *Atmospheric Environment*, *8*, 1251–1256.

Vinoj, V., Rasch, P. J., Wang, H., Yoon, J. H., Ma, P. L., Landu, K., & Singh, B. (2014). Short-term modulation of Indian summer monsoon rainfall by West Asian dust. *Nature Geoscience*, *7*(4), 308–313. https://doi.org/10.1038/ngeo2107

Wang, Y., Jiang, J. H., & Su, H. (2015). Atmospheric responses to the redistribution of anthropogenic aerosols. *Journal of Geophysical Research: Atmospheres*, *120*, 9625–9641. https://doi.org/10.1002/2015JD023665

Yin, C., Wang, T., Solmon, F., Mallet, M., Jiang, F., Shu, L., & Zhuang, B. (2015). Assessment of direct radiative forcing due to secondary organic aerosol over China with a regional climate model. *Tellus B*, *1*, 1–19. https://doi.org/10.3402/tellusb.v67.24634

Zakey, A. S., Giorgi, F., & Bi, X. (2008). Modeling of sea salt in a regional climate model: Fluxes and radiative forcing. *Journal of Geophysical Research*, *113*, D14221. https://doi.org/10.1029/2007JD009209

Zakey, A. S., Solmon, F., & Giorgi, F. (2006). Development and testing of a desert dust module in a regional climate model. *Atmospheric Chemistry and Physics*, *6*, 4687–4704.

Zanis, P., Ntogras, C., Zakey, A., Pytharoulis, I., & Karacostas, T. (2012). Regional climate feedback of anthropogenic aerosols over Europe using RegCM3. *Climate Research*, *52*(1), 267–278. https://doi.org/10.3354/cr01070

Zender, C. S., H. Bian, and D. Newman (2003). Mineral Dust Entrainment and Deposition (DEAD) model: Description and 1990s dust climatology, 108. https://doi.org/10.1029/2002JD002775

Zeng, X., Zhao, M., & Dickinson, R. E. (1998). Intercomparison of bulk aerodynamic algorithms for the computation of sea surface fluxes using toga coare and tao data. *Journal of Climate*, *11*, 2628–2644.

Zhao, A. D., Stevenson, D. S., & Bollasina, M. A. (2019). The role of anthropogenic aerosols in future precipitation extremes over the Asian Monsoon Region. *Climate Dynamics*, *52*(9-10), 6257–6278. https://doi.org/10.1007/s00382-018-4514-7

Zhao, Y., Nielsen, C. P., Lei, Y., Mcelroy, M. B., & Hao, J. (2011). Quantifying the uncertainties of a bottom-up emission inventory of anthropogenic atmospheric pollutants in China. *Atmos Chem Physiologie*, *2295–2308*. https://doi.org/10.5194/acp-11-2295-2011